

Transport-Coupled Bayesian Flows for Molecular Graph Generation

Yida Xiong¹, Jiameng Chen¹, Kun Li¹, Hongzhi Zhang¹,
Xiantao Cai¹, Jia Wu², Wenbin Hu^{1,3,*},

¹School of Computer Science, Wuhan University, Wuhan, China

²Department of Computing, Macquarie University, Sydney, Australia

³Wuhan University Shenzhen Research Institute, Shenzhen, China

*Corresponding author

{yidaxiong, jiameng.chen, likun98, zhanghongzhi, caixiantao, hwb}@whu.edu.cn, jia.wu@mq.edu.au

Abstract

Molecular graph generation (MGG) is essentially a multi-class generative task, aimed at predicting categories of atoms and bonds under strict chemical and structural constraints. However, many prevailing diffusion paradigms learn to regress numerical embeddings and rely on a hard discretization rule during sampling to recover discrete labels. This introduces a fundamental discrepancy between training and sampling. While models are trained for point-wise numerical fidelity, the sampling process fundamentally relies on crossing categorical decision boundaries. This discrepancy forces the model to expend efforts on intra-class variations that become irrelevant after discretization, ultimately compromising diversity, structural statistics, and generalization performance. Therefore, we propose **TopBF**, a unified framework that (i) performs MGG directly in continuous parameter distributions, (ii) learns graph-topological understanding through a Quasi-Wasserstein optimal-transport coupling under geodesic costs, and (iii) supports controllable, property-conditioned generation during sampling without retraining the base model. TopBF innovatively employs cumulative distribution function (CDF) to compute category probabilities induced by the Gaussian channel, thereby unifying the training objective with the sampling discretization operation. Experiments on QM9 and ZINC250k demonstrate superior structural fidelity and efficient generation with improved performance.

1 Introduction

Molecular graph generation (MGG) is a critical yet challenging endeavor in modern computational drug discovery [Li *et al.*, 2025a], facilitating the advancement of downstream tasks such as molecular optimization [Zhu *et al.*, 2023; Xiong *et al.*, 2026] and drug-target binding affinity prediction [Wu *et al.*, 2024; Li *et al.*, 2025b]. Early computational approaches utilizing deep learning attempted to generate molecular graphs in a one-shot manner [Zang and Wang, 2020;

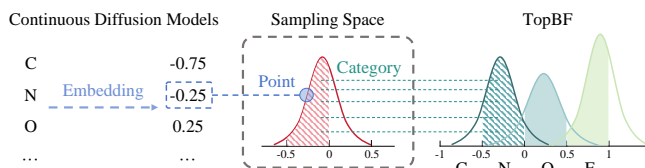


Figure 1: Continuous diffusion models are agnostic of the discretization process and only pursue numerical fitting during training, while TopBF directly calculates the probability of each category.

Kong *et al.*, 2022]. However, these methods often struggle to model complex structures effectively. In recent years, diffusion models have demonstrated remarkable performance across various generation tasks [Gong *et al.*, 2024; Chen *et al.*, 2025]. These models are generally divided into discrete and continuous types and have been progressively integrated into molecular graph generation.

Naturally suited for discrete graph structures, discrete diffusion models typically define a forward Markov process that corrupts the graph structure through discrete edits. Conversely, the reverse process learns to restore the graph by framing generation as an iterative classification task [Vignac *et al.*, 2023; Xu *et al.*, 2024]. However, these discrete diffusion models sacrifice the smoother optimization and dynamic generation afforded by continuous representations. Continuous diffusion models have also demonstrated success in this domain [Jo *et al.*, 2022; Luo *et al.*, 2023]. They operate on a continuous representation of a graph, involving a forward noising process that incrementally perturbs this representation with continuous noise while training a core network to reverse this corruption. The primary objective of continuous diffusion models is to predict embedded representations in continuous space and train a neural network to regress those values under injected noise. However, the final output must be discretized by rounding, which is not a benign post-processing step. As shown in Figure 1, it is evident that throughout the entire training phase, these models remain agnostic regarding the discretization rule. The resulting mismatch between training and sampling can lead to inefficient learning and brittle generation. In particular, point-wise regression errors near category boundaries may be penalized mildly during training but induce catastrophic category flips

at inference, which is especially problematic for generation.

Recently, Bayesian Flow Networks (BFNs) [Graves *et al.*, 2023; Song *et al.*, 2024] provide an alternative paradigm for discrete generation by evolving distribution parameters through a continuous-time Bayesian updating process. Instead of directly predicting discrete values, BFNs propagate a parameter state that represents uncertainty and update it via pseudo-observations, yielding a continuous and differentiable learning process for discrete data. However, BFNs are not topology-aware for molecular graphs, since they adopt independent Gaussian distributions between variables to retain closed-form Bayesian updates. As a result, BFNs are mainly rewarded for getting each position right in isolation, rather than for capturing how labels should cohere with the overall graph structure.

To address the aforementioned issues, we introduce **TopBF**, a molecular graph generative BFN that performs generation in continuous distribution-parameter space and uses a CDF-based decoding to compute category probabilities from continuous parameters, thereby aligning the training objective with the same discretization rule used during sampling. Furthermore, we make TopBF topology-aware by introducing a Quasi-Wasserstein transport coupling defined on graph geodesic costs, which compares predicted categorical mass on atoms and bonds with the ground-truth structure. This geometry-respecting discrepancy encourages local, structure-consistent adjustments and discourages topology-inconsistent long-range rearrangements. TopBF also achieves conditional generation via property-error gradient (PEG) guidance. Notably, TopBF achieves superior performance with the minimum sampling steps, accelerating molecular graph generation in practice. We summarize our key contributions as follows:

- We observe the mismatch defect in continuous diffusion methods and propose TopBF that unifies continuous-parameter training with discrete sampling for MGG.
- We inject topology awareness into TopBF training via a Quasi-Wasserstein transport coupling with graph-geodesic ground costs by aligning predicted categorical mass with the molecular structure in a geometry-consistent manner.
- TopBF supports training-free and property-conditioned generation via guided sampling while requiring the minimum sampling steps, achieving both effective control and efficient MGG.

2 Related Work

Deep generative models for MGG are typically categorized into autoregressive and one-shot models. The former generate graphs incrementally, adding atoms and bonds in an autoregressive manner [You *et al.*, 2018a; You *et al.*, 2018b; Jin *et al.*, 2018; Jin *et al.*, 2020]. The latter generate the entire graph at once [Simonovsky and Komodakis, 2018; Shi *et al.*, 2020; Luo *et al.*, 2021; Martinkus *et al.*, 2022].

Diffusion models have been adapted for molecular graph generation [Liu *et al.*, 2023; Qiu *et al.*, 2023; Li *et al.*, 2024]. Some methods define a diffusion process directly on the discrete state space [Vignac *et al.*, 2023; Xu *et al.*, 2024], which

can be complex to accomplish. Others map discrete attributes to a continuous space and apply standard Gaussian diffusion [Huang *et al.*, 2022; Lee *et al.*, 2023].

BFNs have arisen recently to perform generation in continuous parameter distribution [Graves *et al.*, 2023; Song *et al.*, 2024; Qu *et al.*, 2024]. The process starts with a simple prior distribution and iteratively refines its parameters via Bayesian inference to calculate the posterior from observed samples.

3 Preliminaries

3.1 Problem Definition

A molecular graph G is defined as (X, A) , where $X \in \{1, \dots, K_X\}^D$ represents a matrix of D atom features derived from K_X classes, and $A \in \{1, \dots, K_A\}^{D \times D}$ denotes an adjacency matrix encapsulating bond features from K_A classes. Here D is the maximum number of atoms in the considered molecules and let $N \leq D$ be the number of valid atoms.

Given a dataset $\mathcal{D} = \{G_i\}_{i=1}^{|\mathcal{D}|}$ sampled from an unknown data distribution $p_{\text{data}}(G)$, the goal of molecular graph generation is to learn a generative model $p_{\theta}(G)$ that can efficiently sample valid, diverse molecular graphs whose distribution matches p_{data} in terms of structural and chemical statistics. For the discrete nature of molecular graphs, this task can be seen as a multi-class generative task, where we need to assign specific atomic or chemical bond types at each position subject to chemical validity constraints. In addition, the model may be guided towards desired properties \mathbf{z} to achieve conditional molecular graph generation as a flexible extension.

3.2 Bayesian Flow Networks

Bayesian Flow Networks can be conceptualized as a data transmission protocol between a sender and a receiver. Given data $\mathbf{x} = (x^{(1)}, \dots, x^{(D)})$, let $\boldsymbol{\theta} = (\theta^{(1)}, \dots, \theta^{(D)})$ be the parameters of a factorized *input distribution*: $p_I(\mathbf{x} | \boldsymbol{\theta}) = \prod_{d=1}^D p_I(x^{(d)} | \theta^{(d)})$. At each time $t \in [0, 1]$, the sender corrupts \mathbf{x} by a Gaussian channel α yielding a *sender distribution*: $p_S(\mathbf{y} | \mathbf{x}; \alpha) = \prod_{d=1}^D p_S(y^{(d)} | x^{(d)}; \alpha)$. During the data transmission process, the input parameters $\boldsymbol{\theta}$ are input into a neural network Ψ , whose output is then parameterized as an *output distribution*: $p_O(\mathbf{x} | \boldsymbol{\theta}, t) = \prod_{d=1}^D p_O(x^{(d)} | \Psi(\boldsymbol{\theta}, t))$. Since the receiver knows the form of the sender distribution but does not know \mathbf{x} , it integrates all possible \mathbf{x}' and sender distributions, weighted by the output distribution, and obtains the *receiver distribution*: $p_R(\mathbf{y} | \boldsymbol{\theta}; t, \alpha) = \mathbb{E}_{p_O(\mathbf{x}' | \boldsymbol{\theta}; t)} p_S(\mathbf{y} | \mathbf{x}'; \alpha)$. Subsequently, by applying Bayesian inference, *Bayesian update function* $h(\cdot)$ is derived to repeatedly update the parameters: $\boldsymbol{\theta}' = h(\boldsymbol{\theta}, \mathbf{y}, \alpha)$ along a noise schedule, defined as a continuous-time Bayesian flow $p_F(\boldsymbol{\theta} | \mathbf{x}; t)$. The *Bayesian update distribution* is then defined by marginalizing out \mathbf{y} : $p_U(\boldsymbol{\theta}' | \boldsymbol{\theta}, \mathbf{x}; \alpha) = \mathbb{E}_{p_S(\mathbf{y} | \mathbf{x}; \alpha)} \delta(\boldsymbol{\theta}' - h(\boldsymbol{\theta}, \mathbf{y}, \alpha))$, where $\delta(\cdot)$ is the Dirac delta distribution. Now define the *accuracy schedule* $\beta(t)$ as $\beta(t) = \int_{t'=0}^t \alpha(t') dt'$, and the *Bayesian flow distribution* is the marginal distribution over input parameters at time t : $p_F(\boldsymbol{\theta} | \mathbf{x}; t) = p_U(\boldsymbol{\theta} | \boldsymbol{\theta}_0; \mathbf{x}; \beta(t))$.

3.3 Optimal Transport and Quasi-Wasserstein Coupling on Graphs

Optimal transport (OT) provides a geometry-aware way to compare two distributions by measuring the minimum cost required to move probability mass from one to the other [Gabriel and Marco, 2019]. Consider a molecular graph $G = (X, A)$ with N atoms, and let $C \in \mathbb{R}_+^{N \times N}$ be the geodesic ground-cost matrix induced by the shortest-path metric on G , i.e., $C_{ij} = \text{dist}_G(i, j)$. Given two probability distributions $\mathbf{a}, \mathbf{b} \in \Delta^{N-1}$ over atom indices, the entropically regularized OT cost is $\mathcal{W}_\varepsilon(\mathbf{a}, \mathbf{b}; C) = \min_{P \in \Pi(\mathbf{a}, \mathbf{b})} (P, C) + \varepsilon \sum_{i,j} P_{ij} (\log P_{ij} - 1)$, where $\Pi(\mathbf{a}, \mathbf{b}) = \{P \geq 0 \mid P\mathbf{1} = \mathbf{a}, P^\top \mathbf{1} = \mathbf{b}\}$. In practice, we solve the entropy-regularized OT and obtain the coupling P via Sinkhorn iterations [Cuturi, 2013].

Quasi-Wasserstein (QW) extends this idea from comparing single scalar signals on atoms to comparing multi-class label fields on graphs. Specifically, for a categorical field with K classes, we view the category probability map $P(\cdot, k) \in [0, 1]^N$ as a mass distribution over atom indices for each class k , and compare prediction $P(\cdot, k)$ and target $Q(\cdot, k)$ by transporting mass within each class under the same geodesic cost C . The QW discrepancy then aggregates these per-class transport costs: $\mathcal{D}_{\text{QW}}(P, Q; C) = \frac{1}{K} \sum_{k=1}^K \mathcal{W}_\varepsilon(\mathbf{a}_k, \mathbf{b}_k; C)$, $\mathbf{a}_k = \text{Norm}(P(\cdot, k))$, $\mathbf{b}_k = \text{Norm}(Q(\cdot, k))$, where $\text{Norm}(\cdot)$ denotes normalization to the simplex on valid atoms. In contrast to position-wise divergences, \mathcal{D}_{QW} penalizes errors according to how far probability mass must move along the graph, thereby encouraging local and topology-consistent corrections while discouraging long-range and structure-inconsistent reallocations.

4 Methodology

In this section, we describe how our MGG framework, Transport-Coupled Bayesian Flows (TopBF), generates molecular graphs via Bayesian flows over continuous distribution parameters, as illustrated in Figure 2. Pseudocodes for training and sampling are provided in Appendix H.

4.1 Parameterization of Molecular Graphs

Since directly manipulating discrete data often leads to more complex operations to guarantee differentiability, a foundational step of our method involves mapping the discrete atom and bond features into continuous spaces. For a feature class $k \in \{1, \dots, K\}$, we define a deterministic mapping to a continuous value $x_k \in [-1, 1]$:

$$k_c = \frac{2k-1}{K} - 1, \quad k_l = k_c - \frac{1}{K}, \quad k_r = k_c + \frac{1}{K}, \quad (1)$$

where k_l , k_c and k_r represent the respective vectors for left boundaries, centers and right boundaries of the classes. Importantly, we assign the continuous value $x_k := k_c$ to the k -th class. This mapping transforms the ground-truth graph G into continuous representation $\mathbf{G} = (\mathbf{X}, \mathbf{A})$. This continuous representation serves as the target signal for the generative flow.

4.2 Bayesian Flow Over Distribution Parameters

Input distribution in parameter space.

Instead of modeling G directly as diffusion models, TopBF operate on parameters of a simple input distribution over continuous \mathbf{G} . For each of atoms and bonds we maintain a Gaussian input distribution:

$$p_I(\mathbf{X} \mid \boldsymbol{\theta}_X) = \mathcal{N}(\mathbf{X} \mid \boldsymbol{\mu}_X, \rho_X^{-1} \mathbf{I}), \quad (2)$$

$$p_I(\mathbf{A} \mid \boldsymbol{\theta}_A) = \mathcal{N}(\mathbf{A} \mid \boldsymbol{\mu}_A, \rho_A^{-1} \mathbf{I}), \quad (3)$$

where $\boldsymbol{\theta} \stackrel{def}{=} (\boldsymbol{\mu}, \rho)$ consists of a mean vector $\boldsymbol{\mu} \in \mathbb{R}^D$ and a scalar precision $\rho > 0$, and \mathbf{I} is the $D \times D$ identity matrix. The process initiates with a standard normal prior $p_I(\cdot \mid \boldsymbol{\theta}_0) = \mathcal{N}(\cdot \mid \mathbf{0}, \mathbf{I})$ at time $t = 0$. For brevity, we will use the integrated form in our formulas: $p_I(\mathbf{G} \mid \boldsymbol{\theta}) = \mathcal{N}(\mathbf{G} \mid \boldsymbol{\mu}, \rho^{-1} \mathbf{I})$, except in special circumstances.

Sender distribution: adding noise to the data.

Given continuous $\mathbf{G} = (\mathbf{X}, \mathbf{A})$, the sender distribution plays a role forwarding noising data. For each time-dependent accuracy parameter $\alpha(t)$, the sender draws a noisy message:

$$p_S(\mathbf{Y} \mid \mathbf{G}; \alpha(t)) = \mathcal{N}(\mathbf{Y} \mid \mathbf{G}, \alpha(t)^{-1} \mathbf{I}), \quad (4)$$

where $\mathbf{Y} = (Y^{(1)}, \dots, Y^{(D)})$ is a noisy observation of the true graph, whose noise level increases when $\alpha(t)$ is small.

Bayesian update and Bayesian flow distribution.

BFNs define a Bayesian update that combines the current input distribution $p_I(\mathbf{G} \mid \boldsymbol{\theta})$ with a noisy observation \mathbf{Y} from the sender, yielding a posterior over \mathbf{G} that can again be written as a Gaussian in closed form. Since both p_I and p_S are Gaussians with diagonal covariances, the Bayesian update for each of atoms and bonds reduces to [Murphy, 2007]:

$$\begin{cases} \rho_i = \rho_{i-1} + \alpha, \\ \boldsymbol{\mu}_i = \frac{\rho_{i-1} \boldsymbol{\mu}_{i-1} + \alpha \mathbf{Y}}{\rho_{i-1} + \alpha}. \end{cases} \quad (5)$$

Repeating this update along a schedule of accuracies induces a stochastic trajectory $\{\boldsymbol{\theta}_t\}_{t \in [0,1]}$ in parameter space that converges towards the true graph \mathbf{G} as $t \rightarrow 1$.

Rather than explicitly simulating all intermediate steps, there exists a *Bayesian flow distribution* $p_F(\boldsymbol{\theta} \mid \mathbf{G}; t)$ describing the distribution of input parameters at time t after aggregating all past Bayesian updates, as elaborated in Sec. 3.2.

Conceptually, the dynamics are defined on *distribution parameters* $(\boldsymbol{\mu}, \rho)$ rather than on data itself. This is the key distinction of TopBF from standard diffusion models.

4.3 Output and Receiver Distributions for Molecular Graphs

The core neural network in TopBF takes as input the current parameter state $\boldsymbol{\theta}_t$ and time t , and outputs a prediction of the Gaussian noise used to generate the input mean. We denote the network by:

$$\boldsymbol{\epsilon} = \Psi(\boldsymbol{\theta}_t, \mathbf{c}, t), \quad (6)$$

where \mathbf{c} represents any optional conditioning. The output $\boldsymbol{\epsilon}$ is split into two D -dimensional vectors $(\boldsymbol{\mu}_\epsilon, \ln \boldsymbol{\sigma}_\epsilon)$, which are then transformed into the mean and standard deviation

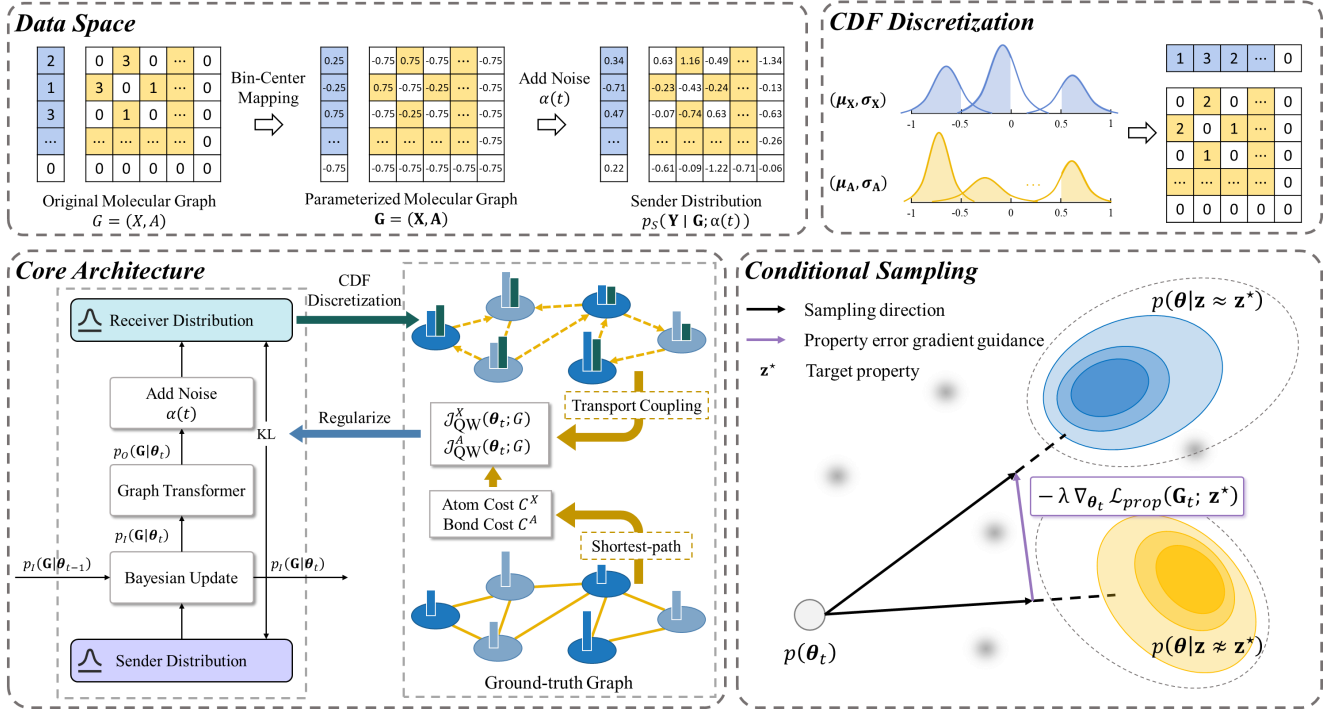


Figure 2: Overall framework of TopBF. **Data Space**: The procedure of parameterizing and adding noise to the molecular graph for the sender distribution. **CDF Discretization**: Obtain atom and bond categories from the output of Ψ through CDF. **Core Architecture**: The structure of a BFN module at time t . And a QW transport coupling regularizes the training procedure. **Conditional Sampling**: PEG guidance for conditional generation.

($\hat{\mu}_{\mathbf{G}}, \hat{\sigma}_{\mathbf{G}}$) of a Gaussian over the continuous data (formal derivation of the transformation in Appendix A):

$$\hat{\mu}_{\mathbf{G}} = \begin{cases} \mathbf{0} & \text{if } t < t_{\min}, \\ \frac{\boldsymbol{\mu}}{\gamma(t)} - \sqrt{\frac{1-\gamma(t)}{\gamma(t)}} \boldsymbol{\mu}_{\epsilon} & \text{otherwise,} \end{cases} \quad (7)$$

$$\hat{\sigma}_{\mathbf{G}} = \begin{cases} \mathbf{1} & \text{if } t < t_{\min}, \\ \sqrt{\frac{1-\gamma(t)}{\gamma(t)}} \exp(\ln \sigma_{\epsilon}) & \text{otherwise,} \end{cases}$$

where $\gamma(t) = \beta(t)/(1 + \beta(t))$ is determined by the accuracy schedule $\beta(t)$ of BFNs, and t_{\min} is a small positive constant to avoid numerical issues at $t = 0$.

Truncated Gaussian CDF and per-class probabilities.

While Eq. (7) defines a continuous Gaussian distribution over \mathbf{G} , our ultimate goal is to make discrete predictions over K classes. To bridge this gap, TopBF uses a truncated Gaussian cumulative distribution function (CDF) to compute the probability mass assigned to each discretization class.

For each dimension $d \in \{1, \dots, D\}$ we define the Gaussian CDF:

$$F(x | \mu_x^{(d)}, \sigma_x^{(d)}) = \frac{1}{2} \left[1 + \operatorname{erf} \left(\frac{x - \mu_x^{(d)}}{\sqrt{2}\sigma_x^{(d)}} \right) \right], \quad (8)$$

where $\operatorname{erf}(\cdot)$ is the error function defined as $\operatorname{erf}(u) = \frac{2}{\sqrt{\pi}} \int_0^u e^{-t^2} dt$. Here truncate the support to the interval

$[-1, 1]$ to align with the embedding range:

$$\mathcal{F}(x | \mu_x^{(d)}, \sigma_x^{(d)}) = \begin{cases} 0 & \text{if } x \leq -1, \\ 1 & \text{if } x \geq 1, \\ F(x | \mu_x^{(d)}, \sigma_x^{(d)}) & \text{otherwise,} \end{cases} \quad (9)$$

Using the class boundaries (k_l, k_r) from Eq. (1), the probability of assigning dimension d to category $k \in \{1, \dots, K\}^D$ is determined by the integral of the truncated Gaussian over the corresponding class:

$$p_O^{(d)}(k | \boldsymbol{\theta}_t) = \mathcal{F}(k_r | \mu_x^{(d)}, \sigma_x^{(d)}) - \mathcal{F}(k_l | \mu_x^{(d)}, \sigma_x^{(d)}). \quad (10)$$

To achieve closed-form *Bayesian update*, the output distribution over the \mathbf{G} is independent across dimensions:

$$p_O(\mathbf{G} | \boldsymbol{\theta}_t) = \prod_{d=1}^D p_O^{(d)}(k(\mathbf{G}^{(d)}) | \boldsymbol{\theta}_t), \quad (11)$$

where $k(x^{(d)})$ denotes the index of the class occupied by $x^{(d)}$. Similarly, we define the expected class-center representation under the current output distribution as:

$$\mathbb{E}[P(\boldsymbol{\theta}, t)] = \hat{\mathbf{k}}(\boldsymbol{\theta}, t) \stackrel{\text{def}}{=} \left(\sum_{k=1}^K p^{(1)}(k | \boldsymbol{\theta}, t) k_c, \dots, \sum_{k=1}^K p^{(D)}(k | \boldsymbol{\theta}, t) k_c \right). \quad (12)$$

Receiver distribution as a mixture of Gaussians.

The receiver distribution p_R inverts the sender process in parameter space by describing the distribution over noisy messages \mathbf{Y} implied by the current parameter state $\boldsymbol{\theta}_t$. Consequently, substituting Eqs. (4) and (10) into the BFN formulation yields a mixture of Gaussians:

$$p_R(\mathbf{Y} | \boldsymbol{\theta}; t, \alpha(t)) = \mathbb{E}_{p_O(\mathbf{G} | \boldsymbol{\theta}_t)} p_S(\mathbf{Y} | \mathbf{G}; \alpha(t)),$$

$$= \prod_{d=1}^D \sum_{k=1}^K p_O^{(d)}(k | \boldsymbol{\theta}_t) \mathcal{N}(\mathbf{Y}^{(d)} | k_e, \alpha(t)^{-1}). \quad (13)$$

The receiver plays the role of the *reverse* channel in the flow. During training, we encourage the receiver distribution to match the sender distribution applied to \mathbf{G} , while during sampling it serves to generate pseudo-observations that drive the Bayesian updates in Eq. (5). Notably, TopBF applies the above construction independently to atoms and bonds by using $K = K_X$ and $K = K_A$, respectively.

4.4 Topology-aware Optimal Transport Matching

Although the position-wise factorization in Eq. (11) enables closed-form Bayesian updates, it also yields largely local and index-wise supervision that does not explicitly encode graph topology. However, categorical errors are not equally severe, since swapping mass within a local neighborhood is structurally less disruptive than relocating it across distant substructures [Frogner *et al.*, 2015; Cheng and Xu, 2024]. To bridge this gap, we introduce an OT coupling that regularizes predictions under molecule’s intrinsic geometry.

Graph-induced Ground Cost.

We define the atom-level ground cost by the shortest-path metric:

$$C_{ij}^X = \text{dist}_G(i, j), \quad i, j \in \{1, \dots, N\}. \quad (14)$$

For bonds, we define an bond-level cost C^A using an endpoint-based proxy consistent with our implementation, e.g., for two undirected bonds $e = (i, j)$ and $e' = (u, v)$,

$$C_{e,e'}^A = \min \{ \text{dist}_G(i, u), \text{dist}_G(i, v), \text{dist}_G(j, u), \text{dist}_G(j, v) \}. \quad (15)$$

Theorem 1 (Endpoint proxy matches line-graph geodesics). *Let $\mathcal{L}(G)$ be the line graph of G whose vertices correspond to bonds and edges connect bonds that share an endpoint. For any two distinct undirected bonds e, e' ,*

$$\text{dist}_{\mathcal{L}(G)}(e, e') = 1 + C_{e,e'}^A.$$

Thus, C^A differs from the exact line-graph geodesic only by an additive constant and induces the same optimal OT coupling (proof in Appendix C).

Optimal Transport over Categorical Mass.

We make topology awareness a first-class objective by minimizing the transport work needed to align predicted categorical mass with the ground truth [Peyré *et al.*, 2016]. At time t , a sample $\boldsymbol{\theta}_t \sim p_F(\boldsymbol{\theta} | \mathbf{G}; t)$ yields categorical probabilities from Eq. (11), with targets Q_X, Q_A . We form class-wise mass fields by normalizing $P_X(\cdot, k)$ and $P_A(\cdot, k)$ on

valid indices and only aggregate over classes that appear in the true graph G : $\mathcal{K}_X^+(G) = \{k \mid \exists i \text{ s.t. } X_i = k\}$ and $\mathcal{K}_A^+(G) = \{k \mid \exists e \text{ s.t. } A_e = k\}$. Thus we define the QW transport costs

$$\mathcal{J}_{\text{QW}}^X(\boldsymbol{\theta}_t; G) = \frac{1}{|\mathcal{K}_X^+(G)|} \sum_{k \in \mathcal{K}_X^+(G)} \mathcal{W}_\varepsilon(\mathbf{a}_k^X, \mathbf{b}_k^X; C^X), \quad (16)$$

$$\mathcal{J}_{\text{QW}}^A(\boldsymbol{\theta}_t; G) = \frac{1}{|\mathcal{K}_A^+(G)|} \sum_{k \in \mathcal{K}_A^+(G)} \mathcal{W}_\varepsilon(\mathbf{a}_k^A, \mathbf{b}_k^A; C^A), \quad (17)$$

where \mathcal{W}_ε is the entropic OT cost in Sec. 3.3; for bonds we exclude the invalid bond class from $\mathcal{K}_A^+(G)$ to avoid trivial domination. The overall training objective then minimizes the expected transport work induced by the receiver predictions,

Theorem 2 (Hard-label limit of class-wise transport). *Fix a class k and suppose $\mathbf{a}_k = \frac{1}{r} \sum_{\ell=1}^r \mathbf{e}_{i_\ell}$ and $\mathbf{b}_k = \frac{1}{r} \sum_{\ell=1}^r \mathbf{e}_{j_\ell}$ are uniform sums of r Diracs. Then*

$$\mathcal{W}_0(\mathbf{a}_k, \mathbf{b}_k; C) = \frac{1}{r} \min_{\pi \in \mathfrak{S}_r} \sum_{\ell=1}^r C_{i_\ell, j_{\pi(\ell)}}.$$

Proof is in Appendix D.2.

4.5 Training Objective

The BFN loss can be interpreted either as the number of nats required to transmit the data through the Bayesian flow, or equivalently as the negative variational lower bound over message sequences. Concretely, we sample $t \sim \mathcal{U}(0, 1)$ and $\boldsymbol{\theta}_t \sim p_F(\boldsymbol{\theta} | \mathbf{G}; t)$, and minimize the expected divergence between the sender distribution applied to the ground-truth discretized graph and the receiver distribution implied by $\boldsymbol{\theta}_t$:

$$\mathcal{L}_G = \mathbb{E}_{t, \boldsymbol{\theta}_t} \left[\text{KL} \left(p_S(\mathbf{Y} | \mathbf{G}; \alpha(t)) \parallel p_R(\mathbf{Y} | \boldsymbol{\theta}_t; t, \alpha(t)) \right) \right]. \quad (18)$$

In TopBF, p_S and p_R are Gaussians with diagonal covariance and we adopt the accuracy schedule $\alpha(t) = \sigma_1^{-2t}$. For a single continuous feature, it makes the KL divergence proportional to a squared error between the true value and the receiver mean. For discretized atom and bond features, we represent each category by k_e in the one-dimensional continuous space and use the expectation of these centers under p_O . Here it yields the continuous-time losses for atoms and bonds (Appendix B for a detailed derivation):

$$\mathcal{L}_X = -\ln \sigma_1 \mathbb{E}_{t \sim \mathcal{U}(0,1), p_F(\boldsymbol{\theta} | \mathbf{X}; t)} \left[\frac{\|\mathbf{X} - \hat{\mathbf{k}}_X(\boldsymbol{\theta}, t)\|_2^2}{\sigma_1^{2t}} \right], \quad (19)$$

where σ_1 is the target standard deviation of the input distribution at $t = 1$. An analogous loss \mathcal{L}_A is defined for bond features and the base objective is $\mathcal{L}_G = \mathcal{L}_X + \mathcal{L}_A$.

To inject explicit topology awareness into training, we further minimize the expected Quasi-Wasserstein transport work defined in Sec. 4.4:

$$\mathbb{E}_{t \sim \mathcal{U}(0,1), \boldsymbol{\theta}_t \sim p_F(\boldsymbol{\theta} | \mathbf{G}; t)} \left[\mathcal{J}_{\text{QW}}^X(\boldsymbol{\theta}_t; \mathbf{G}) + \mathcal{J}_{\text{QW}}^A(\boldsymbol{\theta}_t; \mathbf{G}) \right]. \quad (20)$$

This joint objective preserves the original Bayesian flow formulation while encouraging predictions that align with the ground-truth graph through low-cost geodesic transport.

Method	QM9 ($ N \leq 9$)				ZINC250k ($ N \leq 38$)				Sampling Steps
	Valid(%) \uparrow	Unique \uparrow	FCD \downarrow	NSPDK \downarrow	Valid(%) \uparrow	Unique \uparrow	FCD \downarrow	NSPDK \downarrow	
EDP-GNN	47.52	<u>99.25</u>	2.680	0.0046	82.97	99.79	16.737	0.0485	1000
GDSS	95.72	98.46	2.900	0.0033	97.01	99.64	14.656	0.0195	1000
DiGress	98.19	96.20	<u>0.095</u>	0.0003	94.99	99.97	3.482	0.0021	500
LGD-large	99.13	96.82	0.104	<u>0.0002</u>	-	-	-	-	1000
GruM	<u>99.69</u>	96.90	0.108	<u>0.0002</u>	98.65	99.97	2.257	0.0015	1000
DeFoG	99.30	96.30	0.120	-	99.22	<u>99.99</u>	<u>1.425</u>	0.0008	1000
SID	99.67	95.66	0.504	0.0001	99.50	99.84	2.010	0.0021	500
TopBF	99.74	99.27	0.093	<u>0.0002</u>	<u>99.37</u>	100.00	1.392	0.0008	200

Table 1: Performance comparison on QM9 and ZINC250k datasets. The best results are highlighted in **bold** and the second best are underlined. Null values (-) in criteria indicate that statistics are unavailable from the original paper.

Target	$\mu \downarrow$	HOMO \downarrow	μ & HOMO \downarrow
Unconditional	1.69 \pm 0.05	0.96 \pm 0.01	1.73 \pm 0.02
$\lambda = 0.5$	0.92 \pm 0.04	0.71 \pm 0.02	0.93 \pm 0.03
+PEG $\lambda = 1.0$	0.63 \pm 0.04	0.51 \pm 0.01	0.77 \pm 0.03
$\lambda = 1.5$	1.55 \pm 0.07	0.83 \pm 0.03	1.29 \pm 0.06

Table 2: Comparison on mean absolute error (MAE) between unconditional generation and PEG guidance generation.

4.6 Conditional Generation

TopBF supports conditional generation without retraining the unconditional flow model. Integrating property control via classifier-free [Ho and Salimans, 2021] or regressor-free [Li *et al.*, 2024] guidance often necessitates retraining models from scratch for each target property, which limits their flexibility across different tasks. Instead, we train a separate regressor and apply property-error gradient (PEG) guidance during sampling, which remains flexible for changing targets or composing multiple objectives.

Let $\mathcal{D}_{\text{prop}} = \{(G_i, \mathbf{z}_i)\}_{i=1}^M$ be a property-labeled dataset with property $\mathbf{z} \in \mathbb{R}^{d_z}$. We train a lightweight regressor R_φ on noisy graphs produced by the same sender corruption used in TopBF so that the regressor predicts the clean property from noisy inputs:

$$\hat{\mathbf{z}}_t = R_\varphi(\mathbf{X}_t, \mathbf{A}_t, t), \quad (21)$$

$$\mathcal{L}_{\text{reg}} = \mathbb{E}_{(G, \mathbf{z}) \sim \mathcal{D}_{\text{prop}}} \mathbb{E}_{t \sim \mathcal{U}(0,1)} \mathbb{E}_{\mathbf{Y} \sim p_S(\cdot | G; \alpha(t))} [\|\hat{\mathbf{z}}_t - \mathbf{z}\|_2^2]. \quad (22)$$

Consequently, R_φ learns to estimate properties consistently along the BFN corruption path.

During sampling, we aim to obtain molecules with property close to specified target \mathbf{z}^* . Given the current expected class centers under $p_O(\cdot | \theta_t)$, we compute $\hat{\mathbf{z}}_t = R_\varphi(\mathbf{G}_t, t)$ and define a property error:

$$\mathcal{L}_{\text{prop}}(\mathbf{G}_t; \mathbf{z}^*) = \|\hat{\mathbf{z}}_t - \mathbf{z}^*\|_2^2. \quad (23)$$

Before applying the Bayesian update, we take a small gradient step in parameter space

$$\tilde{\theta}_t = \theta_t - \lambda \nabla_{\theta_t} \mathcal{L}_{\text{prop}}(\mathbf{G}_t; \mathbf{z}^*), \quad (24)$$

where $\lambda \geq 0$ controls the guidance strength and $\lambda = 0$ recovers the unconditional sampling.

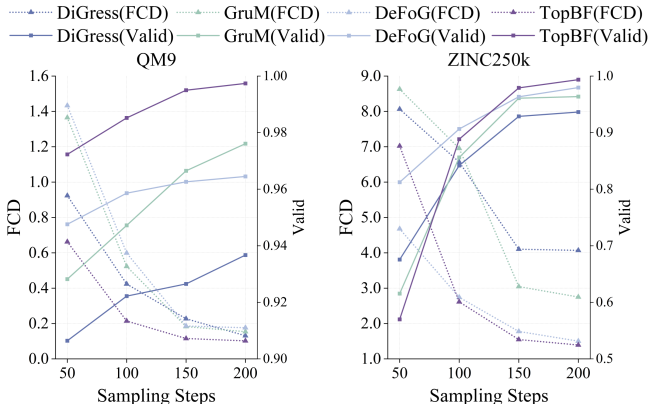


Figure 3: Sampling efficiency comparison between TopBF and baselines on QM9 and ZINC250k datasets.

5 Experiment

We experimentally validate the performance of our method in molecular graph generation task as well as sampling efficiency comparison against representative baselines.

5.1 Experimental Setup

Datasets and Evaluation Metrics

We choose QM9 [Ramakrishnan *et al.*, 2014] and ZINC250k [Irwin *et al.*, 2012] for molecular graph generation, with the evaluation setting following [Jo *et al.*, 2022]: Validity without correction and uniqueness on 10,000 generated molecules. Fréchet ChemNet Distance (FCD) [Preuer *et al.*, 2018] measures the distance between training and generated sets using the activations from the penultimate layer of the ChemNet. Additionally, Neighborhood Subgraph Pairwise Distance Kernel (NSPDK) maximum mean discrepancy (MMD) [Costa and De Grave, 2010] evaluates the MMD between the generated molecules and test molecules which takes into account both the atom and bond features for evaluation.

Baselines

We compare our model against several excellent baselines in MGG. EDP-GNN [Niu *et al.*, 2020] models graphs with a permutation invariant approach. GDSS [Jo *et al.*, 2022] is a score-based diffusion model. DiGress [Vignac *et al.*,

QW on		QM9 ($ N \leq 9$)				ZINC250k ($ N \leq 38$)			
Atoms	Bonds	Valid(%) \uparrow	Unique \uparrow	FCD \downarrow	NSPDK \downarrow	Valid(%) \uparrow	Unique \uparrow	FCD \downarrow	NSPDK \downarrow
x	x	98.63	97.85	0.143	0.0003	94.75	99.03	3.959	0.0031
✓	x	98.79	99.13	<u>0.102</u>	0.0003	95.61	100.00	1.347	0.0011
x	✓	99.81	99.05	0.107	0.0002	99.33	99.99	2.016	<u>0.0009</u>
✓	✓	<u>99.74</u>	99.27	0.093	0.0002	99.37	100.00	<u>1.392</u>	0.0008

Table 3: Ablation study on Quasi-Wasserstein transport coupling. The best results are highlighted in **bold** and the second best are underlined.

2023] generates graphs using a discrete diffusion process. LGD [Zhou *et al.*, 2024] provides a unified framework for all-level graph generation and prediction via latent diffusion. GruM [Jo *et al.*, 2024] models the generative process as a mixture of endpoint-conditioned diffusion. DeFoG [Qin *et al.*, 2025] using a discrete flow matching framework that defines continuous-time probability paths over categorical attributes. SID [Boget, 2025] assumes conditional independence between intermediate states to simplify discrete diffusion.

5.2 Molecular Graph Generation

In our experiments, TopBF demonstrates superior performance for most metrics on both QM9 and ZINC250k, as shown in Table 1, outperforming previous flow-based, flow matching, and diffusion models. Specifically, overall leading on FCD and NSPDK indicate the molecules generated by TopBF closely align with the distributions of the relevant molecular datasets. Furthermore, the highest score on uniqueness manifests the best diversity performance and exploration capability during generation, which further highlights the deficiency of the methods treating training objective as a regression task. Since all methods attain 100% validity after molecular correction, recent methods including TopBF meet industrial requirements. Additionally, Table 1 reveals that TopBF achieves superior effects with significantly fewer sampling steps. We also present randomly selected molecular samples in Appendix G for visualization.

5.3 Conditional Generation

We assess the controllability of TopBF on QM9 by conditioning on graph-level properties, following the setting of DiGress [Vignac *et al.*, 2023]. From the QM9 test split we randomly select 100 molecules, record their dipole moment μ and HOMO energy, and use each pair (μ^*, HOMO^*) as a target. For every target we generate 10 molecules unconditionally and conditionally with PEG guidance, respectively. μ and HOMO are computed with Psi4 [Smith *et al.*, 2020] from conformers built with RDKit¹, and mean absolute error (MAE) is reported between the targets and the estimated properties for above three tasks. We also carry out sensitivity analysis on λ . As shown in Table 2, TopBF with PEG guidance consistently yields lower MAE than the unconditional sampler, demonstrating effective property control. PEG with $\lambda = 1.0$ performs best, as we infer that $\lambda = 0.5$ guides little during sampling and guidance strength with $\lambda = 1.5$ invades

the original gradient to generate valid molecules, affecting the property values conversely.

5.4 Sampling Efficiency and Effect

We conduct a sampling efficiency experiment to compare the sampling velocity against representative baselines. As manifested in Figure 3, our method exhibits exceptional performance during initial 100 steps. Scores could be further improved if sampling with steps longer than 200. However, we choose 200 steps as the best accuracy-efficiency trade-off. This characteristic renders TopBF well-suited for generating high-quality molecular samples while maintaining competitive in inference time.

5.5 Ablation on Quasi-Wasserstein Coupling

We further conduct an ablation study to isolate the effect of the proposed QW transport coupling on atom types and bond types. All variants share the same architecture, training schedule, and sampling steps, differing only in whether the topology-aware transport objective is activated on atoms and/or bonds. As reported in Table 3, applying QW to both atoms and bonds achieves the best overall performance. Moreover, the two partial variants reveal complementary behaviors, where enabling QW on atoms mainly enhances distributional fidelity reflected by FCD, while enabling QW on bonds primarily strengthens validity and graph-structural alignment reflected by NSPDK. Removing QW leads to a uniform degradation, indicating that topology-aware transport coupling provides an effective structural learning signal beyond CDF-aligned Bayesian flow objective with the default L_2 regularization, and that jointly coupling atoms and bonds yields the most reliable gains.

6 Conclusion

In this paper, we introduce **TopBF**, a transport-coupled Bayesian Flow framework for molecular graph generation. TopBF operates in continuous parameter distributions and employs a CDF-based output channel to directly compute category probabilities, aligning the training objective with the discrete discretization used during sampling procedure, rather than fitting arbitrary continuous embeddings. To further inject topology awareness without breaking closed-form Bayesian updates, we formulate a Quasi-Wasserstein transport coupling under geodesic costs, encouraging topology-consistent alignment of atom and bond categorical mass on molecular graphs. Empirically, TopBF achieves state-of-the-art results on standard molecular graph generation benchmarks with efficient sampling of the minimum steps.

¹<https://www.rdkit.org>

References

- [Boget, 2025] Yoann Boget. Simple and critical iterative denoising: A recasting of discrete diffusion in graph generation. In *Forty-second International Conference on Machine Learning*, 2025.
- [Chen *et al.*, 2025] Jiameng Chen, Xiantao Cai, Jia Wu, and Wenbin Hu. Antibody design and optimization with multi-scale equivariant graph diffusion models for accurate complex antigen binding. *arXiv preprint arXiv:2506.20957*, 2025.
- [Cheng and Xu, 2024] Minjie Cheng and Hongteng Xu. A quasi-wasserstein loss for learning graph neural networks. In *Proceedings of the ACM Web Conference 2024*, pages 815–826, 2024.
- [Costa and De Grave, 2010] Fabrizio Costa and Kurt De Grave. Fast neighborhood subgraph pairwise distance kernel. In *Proceedings of the 26th International Conference on Machine Learning*, pages 255–262. Omnipress; Madison, WI, USA, 2010.
- [Cuturi, 2013] Marco Cuturi. Sinkhorn distances: Light-speed computation of optimal transport. *Advances in neural information processing systems*, 26, 2013.
- [Dwivedi and Bresson, 2020] Vijay Prakash Dwivedi and Xavier Bresson. A generalization of transformer networks to graphs. *arXiv preprint arXiv:2012.09699*, 2020.
- [Frogner *et al.*, 2015] Charlie Frogner, Chiyuan Zhang, Hossein Mobahi, Mauricio Araya, and Tomaso A Poggio. Learning with a wasserstein loss. *Advances in neural information processing systems*, 28, 2015.
- [Gabriel and Marco, 2019] Peyré Gabriel and Cuturi Marco. Computational optimal transport with applications to data sciences. *Foundations and Trends® in Machine Learning*, 11(5-6):355–607, 2019.
- [Gong *et al.*, 2024] Haisong Gong, Qiang Liu, Shu Wu, and Liang Wang. Text-guided molecule generation with diffusion language model. In *Proceedings of the AAAI Conference on Artificial Intelligence*, volume 38, pages 109–117, 2024.
- [Graves *et al.*, 2023] Alex Graves, Rupesh Kumar Srivastava, Timothy Atkinson, and Faustino Gomez. Bayesian flow networks. *arXiv preprint arXiv:2308.07037*, 2023.
- [Ho and Salimans, 2021] Jonathan Ho and Tim Salimans. Classifier-free diffusion guidance. In *NeurIPS 2021 Workshop on Deep Generative Models and Downstream Applications*, 2021.
- [Huang *et al.*, 2022] Han Huang, Leilei Sun, Bowen Du, Yanjie Fu, and Weifeng Lv. Graphgdp: Generative diffusion processes for permutation invariant graph generation. In *2022 IEEE International Conference on Data Mining (ICDM)*, pages 201–210. IEEE, 2022.
- [Irwin *et al.*, 2012] John J Irwin, Teague Sterling, Michael M Mysinger, Erin S Bolstad, and Ryan G Coleman. Zinc: a free tool to discover chemistry for biology. *Journal of chemical information and modeling*, 52(7):1757–1768, 2012.
- [Jin *et al.*, 2018] Wengong Jin, Regina Barzilay, and Tommi Jaakkola. Junction tree variational autoencoder for molecular graph generation. In *International conference on machine learning*, pages 2323–2332. PMLR, 2018.
- [Jin *et al.*, 2020] Wengong Jin, Regina Barzilay, and Tommi Jaakkola. Hierarchical generation of molecular graphs using structural motifs. In *International conference on machine learning*, pages 4839–4848. PMLR, 2020.
- [Jo *et al.*, 2022] Jaehyeong Jo, Seul Lee, and Sung Ju Hwang. Score-based generative modeling of graphs via the system of stochastic differential equations. In *International conference on machine learning*, pages 10362–10383. PMLR, 2022.
- [Jo *et al.*, 2024] Jaehyeong Jo, Dongki Kim, and Sung Ju Hwang. Graph generation with diffusion mixture. In *Proceedings of the 41st International Conference on Machine Learning*, pages 22371–22405, 2024.
- [Kong *et al.*, 2022] Xiangzhe Kong, Wenbing Huang, Zhixing Tan, and Yang Liu. Molecule generation by principal subgraph mining and assembling. *Advances in Neural Information Processing Systems*, 35:2550–2563, 2022.
- [Lee *et al.*, 2023] Seul Lee, Jaehyeong Jo, and Sung Ju Hwang. Exploring chemical space with score-based out-of-distribution generation. In *International Conference on Machine Learning*, pages 18872–18892. PMLR, 2023.
- [Li *et al.*, 2024] Kun Li, Xiuwen Gong, Shirui Pan, Jia Wu, Bo Du, and Wenbin Hu. Regressor-free molecule generation to support drug response prediction. *arXiv preprint arXiv:2405.14536*, 2024.
- [Li *et al.*, 2025a] Kun Li, Yida Xiong, Hongzhi Zhang, Xiantao Cai, Jia Wu, Bo Du, and Wenbin Hu. Graph-structured small molecule drug discovery through deep learning: Progress, challenges, and opportunities. In *2025 IEEE International Conference on Web Services (ICWS)*, pages 1033–1042, 2025.
- [Li *et al.*, 2025b] Kun Li, Yue Zeng, Yi-da Xiong, Hao-chen Wu, Sui Fang, Zhi-yan Qu, Yan Zhu, Bo Du, Zhao-bing Gao, and Wen-bin Hu. Contrastive learning-based drug screening model for glun1/glun3a inhibitors. *Acta Pharmacologica Sinica*, pages 1–13, 2025.
- [Liu *et al.*, 2023] Chengyi Liu, Wenqi Fan, Yunqing Liu, Jiantong Li, Hang Li, Hui Liu, Jiliang Tang, and Qing Li. Generative diffusion models on graphs: methods and applications. In *Proceedings of the Thirty-Second International Joint Conference on Artificial Intelligence*, pages 6702–6711, 2023.
- [Luo *et al.*, 2021] Youzhi Luo, Keqiang Yan, and Shuiwang Ji. Graphdf: A discrete flow model for molecular graph generation. In *International conference on machine learning*, pages 7192–7203. PMLR, 2021.
- [Luo *et al.*, 2023] Tianze Luo, Zhanfeng Mo, and Sinno Jialin Pan. Fast graph generation via spectral diffusion. *IEEE Transactions on Pattern Analysis and Machine Intelligence*, 46(5):3496–3508, 2023.

- [Martinkus *et al.*, 2022] Karolis Martinkus, Andreas Loukas, Nathanaël Perraudin, and Roger Wattenhofer. Spectre: Spectral conditioning helps to overcome the expressivity limits of one-shot graph generators. In *International Conference on Machine Learning*, pages 15159–15179. PMLR, 2022.
- [Murphy, 2007] Kevin P Murphy. Conjugate bayesian analysis of the gaussian distribution. *def*, 1(2 σ):16, 2007.
- [Niu *et al.*, 2020] Chenhao Niu, Yang Song, Jiaming Song, Shengjia Zhao, Aditya Grover, and Stefano Ermon. Permutation invariant graph generation via score-based generative modeling. In *International conference on artificial intelligence and statistics*, pages 4474–4484. PMLR, 2020.
- [Peyré *et al.*, 2016] Gabriel Peyré, Marco Cuturi, and Justin Solomon. Gromov-wasserstein averaging of kernel and distance matrices. In *International conference on machine learning*, pages 2664–2672. PMLR, 2016.
- [Preuer *et al.*, 2018] Kristina Preuer, Philipp Renz, Thomas Unterthiner, Sepp Hochreiter, and Gunter Klambauer. Fréchet chemnet distance: a metric for generative models for molecules in drug discovery. *Journal of chemical information and modeling*, 58(9):1736–1741, 2018.
- [Qin *et al.*, 2025] Yiming Qin, Manuel Madeira, Dorina Thanou, and Pascal Frossard. Defog: Discrete flow matching for graph generation. In *International Conference on Machine Learning (ICML)*, 2025.
- [Qiu *et al.*, 2023] Ruizhong Qiu, Dingsu Wang, Lei Ying, H Vincent Poor, Yifang Zhang, and Hanghang Tong. Reconstructing graph diffusion history from a single snapshot. In *Proceedings of the 29th ACM SIGKDD Conference on Knowledge Discovery and Data Mining*, pages 1978–1988, 2023.
- [Qu *et al.*, 2024] Yanru Qu, Keyue Qiu, Yuxuan Song, Jingjing Gong, Jiawei Han, Mingyue Zheng, Hao Zhou, and Wei-Ying Ma. Molcraft: Structure-based drug design in continuous parameter space. In *Forty-first International Conference on Machine Learning*, 2024.
- [Ramakrishnan *et al.*, 2014] Raghunathan Ramakrishnan, Pavlo O Dral, Matthias Rupp, and O Anatole Von Lilienfeld. Quantum chemistry structures and properties of 134 kilo molecules. *Scientific data*, 1(1):1–7, 2014.
- [Shi *et al.*, 2020] Chence Shi, Minkai Xu, Zhaocheng Zhu, Weinan Zhang, Ming Zhang, and Jian Tang. Graphaf: a flow-based autoregressive model for molecular graph generation. In *International Conference on Learning Representations*, 2020.
- [Simonovsky and Komodakis, 2018] Martin Simonovsky and Nikos Komodakis. Graphvae: Towards generation of small graphs using variational autoencoders. In *International conference on artificial neural networks*, pages 412–422. Springer, 2018.
- [Smith *et al.*, 2020] Daniel GA Smith, Lori A Burns, Andrew C Simmonett, Robert M Parrish, Matthew C Schieber, Raimondas Galvelis, Peter Kraus, Holger Kruse, Roberto Di Remigio, Asem Alenaizan, et al. Psi4 1.4: Open-source software for high-throughput quantum chemistry. *The Journal of chemical physics*, 152(18), 2020.
- [Song *et al.*, 2024] Yuxuan Song, Jingjing Gong, Hao Zhou, Mingyue Zheng, Jingjing Liu, and Wei-Ying Ma. Unified generative modeling of 3d molecules with bayesian flow networks. In *The Twelfth International Conference on Learning Representations*, 2024.
- [Vignac *et al.*, 2023] Clement Vignac, Igor Krawczuk, Antoine Siraudin, Bohan Wang, Volkan Cevher, and Pascal Frossard. Digress: Discrete denoising diffusion for graph generation. In *The Eleventh International Conference on Learning Representations*, 2023.
- [Wu *et al.*, 2024] Lirong Wu, Yufei Huang, Cheng Tan, Zhangyang Gao, Bozhen Hu, Haitao Lin, Zicheng Liu, and Stan Z Li. Psc-cpi: Multi-scale protein sequence-structure contrasting for efficient and generalizable compound-protein interaction prediction. In *Proceedings of the AAAI conference on artificial intelligence*, volume 38, pages 310–319, 2024.
- [Xiong *et al.*, 2026] Yida Xiong, Kun Li, Jiameng Chen, Hongzhi Zhang, Di Lin, Yan Che, and Wenbin Hu. Text-guided multi-property molecular optimization with a diffusion language model. *Information Fusion*, 127:103907, 2026.
- [Xu *et al.*, 2024] Zhe Xu, Ruizhong Qiu, Yuzhong Chen, Huiyuan Chen, Xiran Fan, Menghai Pan, Zhichen Zeng, Mahashweta Das, and Hanghang Tong. Discrete-state continuous-time diffusion for graph generation. *Advances in Neural Information Processing Systems*, 37:79704–79740, 2024.
- [You *et al.*, 2018a] Jiakuan You, Bowen Liu, Zhitao Ying, Vijay Pande, and Jure Leskovec. Graph convolutional policy network for goal-directed molecular graph generation. *Advances in neural information processing systems*, 31, 2018.
- [You *et al.*, 2018b] Jiakuan You, Rex Ying, Xiang Ren, William Hamilton, and Jure Leskovec. Graphrnn: Generating realistic graphs with deep auto-regressive models. In *International conference on machine learning*, pages 5708–5717. PMLR, 2018.
- [Zang and Wang, 2020] Chengxi Zang and Fei Wang. Moflow: an invertible flow model for generating molecular graphs. In *Proceedings of the 26th ACM SIGKDD international conference on knowledge discovery & data mining*, pages 617–626, 2020.
- [Zhou *et al.*, 2024] Cai Zhou, Xiyuan Wang, and Muhan Zhang. Unifying generation and prediction on graphs with latent graph diffusion. *Advances in Neural Information Processing Systems*, 37:61963–61999, 2024.
- [Zhu *et al.*, 2023] Yiheng Zhu, Jialu Wu, Chaowen Hu, Jiahuan Yan, Tingjun Hou, Jian Wu, et al. Sample-efficient multi-objective molecular optimization with gflownets. *Advances in Neural Information Processing Systems*, 36:79667–79684, 2023.

A Derivation of Eq. (7)

We derive how the network outputs $(\boldsymbol{\mu}_\epsilon, \ln \boldsymbol{\sigma}_\epsilon)$ are mapped to the mean and standard deviation $(\boldsymbol{\mu}_\mathbf{G}, \boldsymbol{\sigma}_\mathbf{G})$ of the Gaussian over \mathbf{G} used in Eq. (7).

Consider one scalar dimension $G^{(d)}$ of the parameterized continuous graph representation \mathbf{G} , and let $\mu_t^{(d)}$ be the corresponding entry of the input mean at time t . From the Bayesian flow over parameters, the marginal distribution of $\mu_t^{(d)}$ conditioned on $G^{(d)}$ is

$$\mu_t^{(d)} | G^{(d)}, t \sim \mathcal{N}(\gamma(t) G^{(d)}, \gamma(t)(1 - \gamma(t))), \quad (25)$$

where $\gamma(t)$ is the function defined in the main text.

Therefore there exists $\epsilon^{(d)} \sim \mathcal{N}(0, 1)$ such that

$$\mu_t^{(d)} = \gamma(t) G^{(d)} + \sqrt{\gamma(t)(1 - \gamma(t))} \epsilon^{(d)}. \quad (26)$$

Solving for $G^{(d)}$ gives

$$G^{(d)} = \frac{\mu_t^{(d)}}{\gamma(t)} - \sqrt{\frac{1 - \gamma(t)}{\gamma(t)}} \epsilon^{(d)}. \quad (27)$$

The core network at time t takes $\boldsymbol{\theta}_t$ and optional conditioning as input and outputs

$$\boldsymbol{\epsilon} = \Psi(\boldsymbol{\theta}_t, \mathbf{c}, t), \quad (28)$$

which is split into two D -dimensional vectors $(\boldsymbol{\mu}_\epsilon, \ln \boldsymbol{\sigma}_\epsilon)$. For each dimension d we model the noise as

$$\begin{cases} \epsilon^{(d)} | \boldsymbol{\theta}_t, t \sim \mathcal{N}(\mu_\epsilon^{(d)}, (\sigma_\epsilon^{(d)})^2), \\ \sigma_\epsilon^{(d)} = \exp(\ln \sigma_\epsilon^{(d)}), \end{cases} \quad (29)$$

Substituting this into Eq. (27), we obtain an affine transform of a Gaussian random variable:

$$G^{(d)} | \boldsymbol{\theta}_t, t = \frac{\mu_t^{(d)}}{\gamma(t)} - \sqrt{\frac{1 - \gamma(t)}{\gamma(t)}} \epsilon^{(d)}. \quad (30)$$

If $Z \sim \mathcal{N}(\mu_Z, \sigma_Z^2)$ and $a, b \in \mathbb{R}$, then $a + bZ \sim \mathcal{N}(a + b\mu_Z, b^2\sigma_Z^2)$. Applying this with

$$Z = \epsilon^{(d)}, \quad a = \frac{\mu_t^{(d)}}{\gamma(t)}, \quad b = -\sqrt{\frac{1 - \gamma(t)}{\gamma(t)}},$$

we obtain

$$\begin{cases} G^{(d)} | \boldsymbol{\theta}_t, t \sim \mathcal{N}(\mu_\mathbf{G}^{(d)}, (\sigma_\mathbf{G}^{(d)})^2), \\ \mu_\mathbf{G}^{(d)} = \frac{\mu_t^{(d)}}{\gamma(t)} - \sqrt{\frac{1 - \gamma(t)}{\gamma(t)}} \mu_\epsilon^{(d)}, \\ (\sigma_\mathbf{G}^{(d)})^2 = \frac{1 - \gamma(t)}{\gamma(t)} (\sigma_\epsilon^{(d)})^2, \end{cases} \quad (31)$$

and hence

$$\sigma_\mathbf{G}^{(d)} = \sqrt{\frac{1 - \gamma(t)}{\gamma(t)}} \sigma_\epsilon^{(d)} = \sqrt{\frac{1 - \gamma(t)}{\gamma(t)}} \exp(\ln \sigma_\epsilon^{(d)}). \quad (32)$$

Stacking over all dimensions $d = 1, \dots, D$ and fixing $\boldsymbol{\mu}_\mathbf{G} = \mathbf{0}$, $\boldsymbol{\sigma}_\mathbf{G} = \mathbf{1}$ to avoid numerical issues when $\gamma(t)$ is extremely small, we yields:

$$\begin{aligned} \boldsymbol{\mu}_\mathbf{G} &= \begin{cases} \mathbf{0} & \text{if } t < t_{\min}, \\ \frac{\boldsymbol{\mu}}{\gamma(t)} - \sqrt{\frac{1 - \gamma(t)}{\gamma(t)}} \boldsymbol{\mu}_\epsilon & \text{otherwise,} \end{cases} \\ \boldsymbol{\sigma}_\mathbf{G} &= \begin{cases} \mathbf{1} & \text{if } t < t_{\min}, \\ \sqrt{\frac{1 - \gamma(t)}{\gamma(t)}} \exp(\ln \boldsymbol{\sigma}_\epsilon) & \text{otherwise.} \end{cases} \end{aligned} \quad (33)$$

B From KL flow loss to squared-error objective

Let $\mathbf{X} \in \mathbb{R}^D$ be the continuous parameterization of the atom features of a graph G (the bond case is analogous), and let $\mathbf{Y} \in \mathbb{R}^D$ denote the noisy message received from the sender. The continuous-time flow objective used by TopBF on \mathbf{X} is

$$\mathcal{L}_{\text{flow}}(\mathbf{X}) = \int_0^1 \mathbb{E}_{\boldsymbol{\theta}_t \sim p_F(\boldsymbol{\theta}|\mathbf{X};t)} \left[D_{\text{KL}}(p_S(\mathbf{Y} | \mathbf{X}; \alpha(t)) \| p_R(\mathbf{Y} | \boldsymbol{\theta}_t; t, \alpha(t))) \right] dt. \quad (34)$$

By construction (Sec. 3.2), at each time t the sender and receiver for atoms are Gaussians with the same covariance:

$$p_S(\mathbf{Y} | \mathbf{X}; \alpha(t)) = \mathcal{N}(\mathbf{Y} | \mathbf{X}, \alpha(t)^{-1}\mathbf{I}), \quad (35)$$

$$p_R(\mathbf{Y} | \boldsymbol{\theta}_t; t, \alpha(t)) = \mathcal{N}(\mathbf{Y} | \hat{\mathbf{k}}_{\mathbf{X}}(\boldsymbol{\theta}_t, t), \alpha(t)^{-1}\mathbf{I}), \quad (36)$$

where $\hat{\mathbf{k}}_{\mathbf{X}}(\boldsymbol{\theta}_t, t)$ is the vector of expected bin centres of the output distribution p_O at time t .

For two Gaussians with identical covariance $\Sigma = \alpha^{-1}\mathbf{I}$,

$$\begin{aligned} D_{\text{KL}}(\mathcal{N}(\mathbf{m}_1, \Sigma) \| \mathcal{N}(\mathbf{m}_2, \Sigma)) \\ &= \frac{1}{2}(\mathbf{m}_1 - \mathbf{m}_2)^\top \Sigma^{-1}(\mathbf{m}_1 - \mathbf{m}_2) \\ &= \frac{\alpha}{2} \|\mathbf{m}_1 - \mathbf{m}_2\|_2^2. \end{aligned} \quad (37)$$

Setting $\mathbf{m}_1 = \mathbf{X}$ and $\mathbf{m}_2 = \hat{\mathbf{k}}_{\mathbf{X}}(\boldsymbol{\theta}_t, t)$ and substituting into Eq. (34) gives

$$\mathcal{L}_{\text{flow}}(\mathbf{X}) = \frac{1}{2} \int_0^1 \alpha(t) \mathbb{E}_{\boldsymbol{\theta}_t \sim p_F(\boldsymbol{\theta}|\mathbf{X};t)} [\|\mathbf{X} - \hat{\mathbf{k}}_{\mathbf{X}}(\boldsymbol{\theta}_t, t)\|_2^2] dt. \quad (38)$$

The channel accuracy is parameterized by a monotonically increasing function $\beta(t)$ with $\beta(0) = 0$ and $\beta(1) = \sigma_{1_{\mathbf{X}}}^{-2}$, and

$$\alpha(t) = \frac{d}{dt} \beta(t). \quad (39)$$

We use

$$\beta(t) = \sigma_{1_{\mathbf{X}}}^{-2t} \Rightarrow \alpha(t) = -2 \ln \sigma_{1_{\mathbf{X}}} \sigma_{1_{\mathbf{X}}}^{-2t}. \quad (40)$$

Thus

$$\frac{1}{2} \alpha(t) = -\ln \sigma_{1_{\mathbf{X}}} \sigma_{1_{\mathbf{X}}}^{-2t}, \quad (41)$$

and Eq. (38) becomes

$$\mathcal{L}_{\text{flow}}(\mathbf{X}) = -\ln \sigma_{1_{\mathbf{X}}} \int_0^1 \mathbb{E}_{\boldsymbol{\theta}_t \sim p_F(\boldsymbol{\theta}|\mathbf{X};t)} \left[\frac{\|\mathbf{X} - \hat{\mathbf{k}}_{\mathbf{X}}(\boldsymbol{\theta}_t, t)\|_2^2}{\sigma_{1_{\mathbf{X}}}^{2t}} \right] dt. \quad (42)$$

Writing the integral as an expectation over $t \sim \mathcal{U}(0, 1)$ yields the continuous-time loss

$$\mathcal{L}_{\infty}(\mathbf{X}) = -\ln \sigma_{1_{\mathbf{X}}} \mathbb{E}_{t \sim \mathcal{U}(0,1), \boldsymbol{\theta}_t \sim p_F(\boldsymbol{\theta}|\mathbf{X};t)} \left[\frac{\|\mathbf{X} - \hat{\mathbf{k}}_{\mathbf{X}}(\boldsymbol{\theta}_t, t)\|_2^2}{\sigma_{1_{\mathbf{X}}}^{2t}} \right]. \quad (43)$$

The same derivation for the continuous bond representation \mathbf{A} with its own target scale $\sigma_{1_{\mathbf{A}}}$ gives $\mathcal{L}_{\infty}(\mathbf{A})$; the total training loss is

$$\mathcal{L}_{\mathbf{G}} = \mathcal{L}_{\mathbf{X}} + \mathcal{L}_{\mathbf{A}}.$$

C Proof of Theorem 1

Proof. Let $e = (i, j)$ and $e' = (u, v)$ be two distinct bonds and denote $D := C_{e, e'}^A = \min_{p \in \{i, j\}, q \in \{u, v\}} \text{dist}_G(p, q)$.

$$\text{dist}_{\mathcal{L}(G)}(e, e') \leq |(e, (p_0, p_1), \dots, (p_{D-1}, p_D), e')| \quad (44)$$

$$= D + 1 = 1 + C_{e, e'}^A, \quad (45)$$

where (p_0, \dots, p_D) is a shortest G -path from an endpoint $p_0 \in e$ to an endpoint $p_D \in e'$. For any shortest $\mathcal{L}(G)$ -path $(e = e_0, \dots, e_L = e')$,

$$C_{e, e'}^A = \min_{p \in e, q \in e'} \text{dist}_G(p, q) \leq \text{dist}_G(p_0, p_L) \leq L - 1 = \text{dist}_{\mathcal{L}(G)}(e, e') - 1. \quad (46)$$

Combining yields $\text{dist}_{\mathcal{L}(G)}(e, e') = 1 + C_{e, e'}^A$.

For any coupling Π with total mass 1,

$$\langle \Pi, \text{dist}_{\mathcal{L}(G)} \rangle = \langle \Pi, C^A \rangle + 1, \quad (47)$$

so the additive shift does not change the optimal transport plan. \square

D From Topology Matching to Class-Wise Transport Coupling

This appendix complements Sec. 4.4 by making explicit the optimization principle behind Eqs. (16) and (17). Rather than penalizing misclassification point-wise, we seek the minimum transport cost required to reshape predicted categorical mass into the ground-truth mass along the geodesic geometry of the molecular graph.

Let P_X^t and P_A^t denote the node/bond categorical probabilities induced by θ_t through Eq. (11), and let Q_X, Q_A be the one-hot targets derived from the ground-truth discrete graph. We only couple classes that are present in the target to avoid ill-posed normalization:

$$\mathcal{K}_X^+(G) = \left\{ k \in [K_X] : \sum_{i=1}^N Q_X(i, k) > 0 \right\}, \quad (48)$$

$$\mathcal{K}_A^+(G) = \left\{ k \in [K_A] : \sum_{e \in \mathcal{E}} Q_A(e, k) > 0 \right\}, \quad (49)$$

and for bonds we exclude the no-bond class from $\mathcal{K}_A^+(G)$, as stated in Sec. 4.4.

Let m_X and m_A be the valid masks. For each class k , we form class-wise mass fields on valid indices by simplex normalization:

$$\mathbf{a}_k^X = \text{Norm}(P_X^t(:, k) \odot m_X), \mathbf{b}_k^X = \text{Norm}(Q_X(:, k) \odot m_X), \quad (50)$$

$$\mathbf{a}_k^A = \text{Norm}(P_A^t(:, k) \odot m_A), \mathbf{b}_k^A = \text{Norm}(Q_A(:, k) \odot m_A), \quad (51)$$

where $\text{Norm}(v) = v / \langle \mathbf{1}, v \rangle$ whenever $\langle \mathbf{1}, v \rangle > 0$.

Given the geodesic ground costs C^X and C^A from Eq. (14) and (15), we follow our topology-matching principle that for each semantic class, transport the predicted mass to the target mass with minimum geodesic cost, then aggregate these costs across classes. This yields Eqs. (16) and (17).

D.1 A single optimization view.

The class-wise aggregation admits a clean equivalence to one OT problem on a product space, which clarifies what is being optimized and why it is transport-coupled.

Theorem 3 (Block-diagonal OT equivalence). *Fix $C \in \mathbb{R}_+^{N \times N}$ and $\varepsilon > 0$. Let $\{\mathbf{a}_k\}_{k=1}^K, \{\mathbf{b}_k\}_{k=1}^K \subset \Delta^{N-1}$ be class-wise masses. Define measures on the product index set $[N] \times [K]$ by $\mu(i, k) = \frac{1}{K} \mathbf{a}_k(i)$ and $\nu(i, k) = \frac{1}{K} \mathbf{b}_k(i)$. Consider the cost on the product space:*

$$\bar{C}((i, k), (j, k')) = \begin{cases} C_{ij}, & k = k', \\ +\infty, & k \neq k'. \end{cases} \quad (52)$$

Then the entropic OT objective on the product space decomposes as

$$\mathcal{W}_\varepsilon(\mu, \nu; \bar{C}) = \frac{1}{K} \sum_{k=1}^K \mathcal{W}_\varepsilon(\mathbf{a}_k, \mathbf{b}_k; C). \quad (53)$$

Proof. We prove the decomposition by two chains of inequalities.

$$\mathcal{W}_\varepsilon(\mu, \nu; \bar{C}) = \min_{\Pi \geq 0} \langle \Pi, \bar{C} \rangle + \varepsilon \sum_{(i,k),(j,k')} \Pi_{(i,k),(j,k')} (\log \Pi_{(i,k),(j,k')} - 1) \quad (54)$$

$$\text{s.t.} \quad \sum_{j,k'} \Pi_{(i,k),(j,k')} = \mu(i, k), \quad \sum_{i,k} \Pi_{(i,k),(j,k')} = \nu(j, k').$$

$$\mathcal{W}_\varepsilon(\mu, \nu; \bar{C}) \geq \min_{\substack{\Pi \geq 0 \\ \Pi_{(i,k),(j,k')} = 0, k \neq k'}} \langle \Pi, \bar{C} \rangle + \varepsilon \sum_{(i,k),(j,k')} \Pi_{(i,k),(j,k')} (\log \Pi_{(i,k),(j,k')} - 1) \quad (55)$$

$$= \min_{\{\Pi_k\}_{k=1}^K} \frac{1}{K} \sum_{k=1}^K \left(\langle \Pi_k, C \rangle + \varepsilon \sum_{i,j} (\Pi_k)_{ij} (\log (\Pi_k)_{ij} - 1) \right) - \varepsilon \log K \quad (56)$$

$$\text{s.t.} \quad \Pi_k \geq 0, \Pi_k \mathbf{1} = \mathbf{a}_k, \Pi_k^\top \mathbf{1} = \mathbf{b}_k, \forall k,$$

$$= \frac{1}{K} \sum_{k=1}^K \mathcal{W}_\varepsilon(\mathbf{a}_k, \mathbf{b}_k; C) - \varepsilon \log K. \quad (57)$$

$$\mathcal{W}_\varepsilon(\mu, \nu; \bar{C}) \leq \langle \Pi^*, \bar{C} \rangle + \varepsilon \sum_{(i,k),(j,k')} \Pi_{(i,k),(j,k')}^* (\log \Pi_{(i,k),(j,k')}^* - 1) \quad (58)$$

$$= \frac{1}{K} \sum_{k=1}^K \mathcal{W}_\varepsilon(\mathbf{a}_k, \mathbf{b}_k; C) - \varepsilon \log K, \quad (59)$$

where Π^* is constructed from the class-wise optimizers $\{\Pi_k^*\}$ by

$$\Pi_{(i,k),(j,k')}^* = \frac{1}{K} (\Pi_k^*)_{ij} \mathbf{1}[k = k'].$$

Combining (57)–(59) yields

$$\mathcal{W}_\varepsilon(\mu, \nu; \bar{C}) = \frac{1}{K} \sum_{k=1}^K \mathcal{W}_\varepsilon(\mathbf{a}_k, \mathbf{b}_k; C) - \varepsilon \log K. \quad (60)$$

Since $-\varepsilon \log K$ is a constant independent of $\{\Pi_k\}$, it can be absorbed into the objective without affecting the optimal coupling. Therefore, up to an additive constant,

$$\mathcal{W}_\varepsilon(\mu, \nu; \bar{C}) \equiv \frac{1}{K} \sum_{k=1}^K \mathcal{W}_\varepsilon(\mathbf{a}_k, \mathbf{b}_k; C), \quad (61)$$

which is the stated decomposition. \square

D.2 Proof of Theorem 2

Proof. Fix a class k and consider unregularized OT

$$\mathcal{W}_0(\mathbf{a}_k, \mathbf{b}_k; C) = \min_{\Pi \geq 0} \langle \Pi, C \rangle \quad \text{s.t.} \quad \Pi \mathbf{1} = \mathbf{a}_k, \quad \Pi^\top \mathbf{1} = \mathbf{b}_k. \quad (62)$$

Let $r = \sum_{i=1}^N Q(i, k)$ be the number of valid indices of class k in the target, with $I = \{i_1, \dots, i_r\}$ (predicted locations) and $J = \{j_1, \dots, j_r\}$ (target locations). In the hard-label limit,

$$\mathbf{a}_k = \frac{1}{r} \sum_{\ell=1}^r \mathbf{e}_{i_\ell}, \quad \mathbf{b}_k = \frac{1}{r} \sum_{\ell=1}^r \mathbf{e}_{j_\ell}. \quad (63)$$

The marginal constraints imply $\Pi_{uv} = 0$ unless $(u, v) \in I \times J$; define the restricted matrix $\tilde{\Pi} \in \mathbb{R}_+^{r \times r}$ and cost $\tilde{C} \in \mathbb{R}_+^{r \times r}$ by

$$\tilde{\Pi}_{\ell m} = r \Pi_{i_\ell j_m}, \quad \tilde{C}_{\ell m} = C_{i_\ell j_m}. \quad (64)$$

Then $\tilde{\Pi} \mathbf{1} = \mathbf{1}$ and $\tilde{\Pi}^\top \mathbf{1} = \mathbf{1}$, and

$$\langle \Pi, C \rangle = \sum_{\ell, m} \Pi_{i_\ell j_m} C_{i_\ell j_m} \quad (65)$$

$$= \frac{1}{r} \sum_{\ell, m} \tilde{\Pi}_{\ell m} \tilde{C}_{\ell m} \quad (66)$$

$$= \frac{1}{r} \langle \tilde{\Pi}, \tilde{C} \rangle. \quad (67)$$

Therefore

$$\mathcal{W}_0(\mathbf{a}_k, \mathbf{b}_k; C) = \frac{1}{r} \min_{\tilde{\Pi} \in \mathcal{B}_r} \langle \tilde{\Pi}, \tilde{C} \rangle, \quad \mathcal{B}_r = \{\tilde{\Pi} \geq 0 : \tilde{\Pi} \mathbf{1} = \mathbf{1}, \tilde{\Pi}^\top \mathbf{1} = \mathbf{1}\}. \quad (68)$$

Since the objective is linear, an optimum is attained at an extreme point of \mathcal{B}_r . By Birkhoff–von Neumann [], the extreme points are permutation matrices P_π ($\pi \in \mathfrak{S}_r$), hence

$$\mathcal{W}_0(\mathbf{a}_k, \mathbf{b}_k; C) = \frac{1}{r} \min_{\pi \in \mathfrak{S}_r} \sum_{\ell=1}^r C_{i_\ell, j_{\pi(\ell)}}. \quad (69)$$

Thus, in the hard-label regime, class-wise OT reduces to within-class minimum-cost matching under the geodesic cost C , making long-range permutations strictly more expensive than local corrections. \square

Category	Hyper-parameter	Description	Value
Bayesian Flow	$\sigma_{1,\mathbf{X}}$	The standard deviation of \mathbf{X} of the noise distribution	0.2
	$\sigma_{1,\mathbf{A}}$	The standard deviation of \mathbf{A} of the noise distribution	0.2
	T	Sampling steps	200
	t_{min}	Minimum time	10^{-4}
QW Transport	λ_{QW}	The coefficient weighting the QW structural regularizer	0.1
	ϵ_{QW}	The entropic regularization smoothing the optimal transport plan calculation	0.2
	n_{QW}	The number of Sinkhorn iterations of the entropic Optimal Transport problem	30

Table 4: Hyper-parameters of TopBF.

E Experimental Details

E.1 Datasets

We validate our approach on the QM9 and ZINC250k benchmarks, following the previous experimental setup [Jo *et al.*, 2022]. QM9 contains approximately 133,885 molecules with up to 9 heavy atoms of 4 types, while ZINC250k comprises roughly 249,455 molecules with up to 38 heavy atoms of 9 types, both covering three standard bond types. Adhering to the standard pipeline [Shi *et al.*, 2020; Luo *et al.*, 2021; Jo *et al.*, 2022], molecules undergo kekulization via RDKit, with explicit hydrogens excluded to focus on the heavy-atom graph representation.

E.2 Implementation details

For our TopBF, we train our model with a constant learning rate 10^{-4} with AdamW optimizer and weight decay 10^{-12} , applying the exponential moving average (EMA) to the parameters. The core network $\Psi(\cdot)$ of TopBF is the graph transformer [Dwivedi and Bresson, 2020; Vignac *et al.*, 2023], with the inner parameters consistent across all baselines using it. Other critical hyper-parameters are presented in Table 4.

F Supplementary Experiments

F.1 Computational Efficiency and Wall-Clock Time Analysis

We conduct a rigorous wall-clock time comparison against state-of-the-art baselines. We repeat the measurement and report the average.

Experimental Setup To ensure a fair comparison, all runtime measurements were conducted under a strictly controlled hardware and software environment.

- **Hardware:** All models were trained and evaluated on a single NVIDIA A6000 GPU with an AMD EPYC 7763 (64 cores) @ 2.450GHz CPU.
- **Software:** Experiments were implemented in PyTorch 2.0.1 with CUDA 11.7.
- **Controls:** We fixed the batch size to 1,024 for QM9 and 256 for ZINC250. For sampling efficiency, we measured the total time required to generate 10,000 valid molecules with their own reported sampling steps.

We compare TopBF against three representative baselines: GDSS [Jo *et al.*, 2022], DiGress [Vignac *et al.*, 2023], and SID [Boget, 2025]. These methods represent the current standard for score-based and discrete generative models, respectively.

Method	QM9 (min)↓	ZINC250k (min)↓
GDSS	1.42	26.47
DiGress	10.08	212.95
SID	1.58	25.78
TopBF (Ours)	1.33	23.32

Table 5: Comparison of total sampling time. Lower is better.

As shown in Table 5, TopBF maintains its lead by generating 10,000 valid molecules in just 1.33 minutes for QM9 and 23.32 minutes for ZINC250k. These results indicate that TopBF achieves competitive or improved sampling throughput under our controlled setup. Since QW is used only as a training-time regularizer, it does not introduce additional cost during sampling.

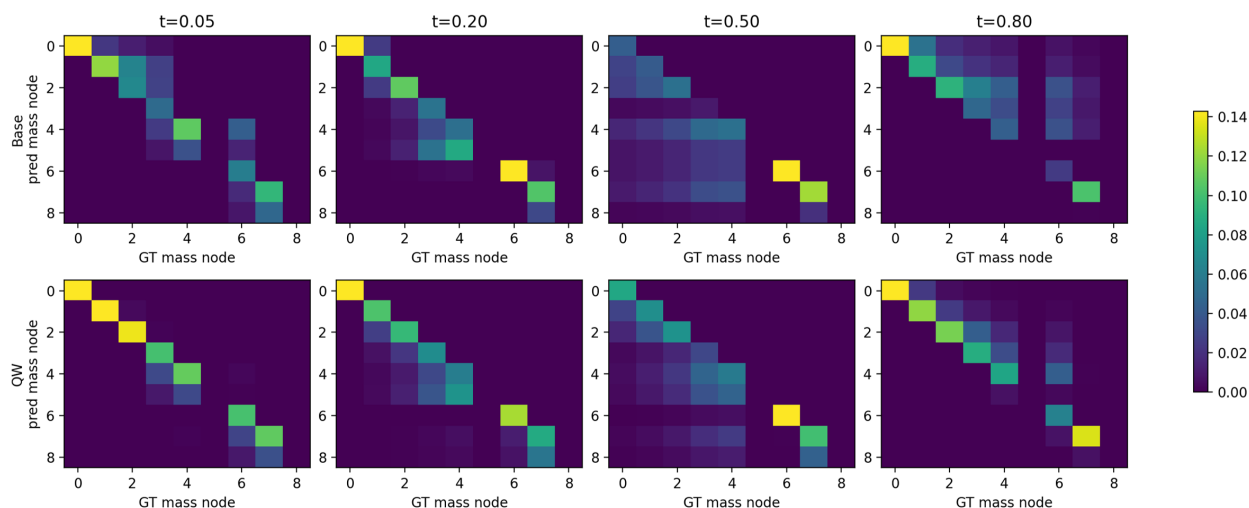


Figure 4: Sinkhorn coupling P between the predicted node-type marginals and the ground truth under the shortest-path (geodesic) cost, probed at $t \in \{0.05, 0.2, 0.5, 0.8\}$ on QM9 dataset.

t	cost_avg↓			localmass1↑			localmass2↑			avg_pX_gt↑		
	Base	QW	Improve	Base	QW	Improve	Base	QW	Improve	Base	QW	Improve
0.05	0.834	0.605	27.5%	0.810	0.852	5.2%	0.911	0.923	1.3%	0.328	0.495	50.9%
0.20	0.815	0.767	5.9%	0.800	0.813	1.6%	0.901	0.911	1.1%	0.347	0.602	73.5%
0.50	1.454	1.149	21.0%	0.612	0.698	14.1%	0.755	0.826	9.4%	0.422	0.581	37.7%
0.80	0.800	0.344	57.0%	0.761	0.913	20.0%	0.913	0.987	8.1%	0.552	0.707	28.1%

Table 6: Probing statistics under shortest-path cost at $t \in \{0.05, 0.2, 0.5, 0.8\}$ (Base vs. QW). QW reduces transport cost and increases local transport mass, indicating more geodesically local corrections.

E.2 Interpretability Analysis

QW regularization is intended to encourage topology-consistent (geodesically local) corrections. To make this effect observable beyond final metrics, we report controlled *probing* at fixed noise levels t . We evaluate four representative noise levels $t \in \{0.05, 0.2, 0.5, 0.8\}$.

For probing, we quantify locality via Sinkhorn-OT diagnostics under shortest-path cost: transport cost $\text{cost_avg}\downarrow$ and local-mass ratios within 1/2 hops $\text{localmass1/2}\uparrow$, together with a correctness proxy $\text{avg_pX_gt}\uparrow$. Improve is relative improvement: for \downarrow , $(\text{Base} - \text{QW})/\text{Base}$; for \uparrow , $(\text{QW} - \text{Base})/\text{Base}$.

Across noise levels, probing verifies the intended mechanism: QW promotes geodesically local corrections (lower cost_avg , higher localmass1/2).

The coupling matrix P transports the predicted node-type mass to the ground-truth mass with graph geodesic distance as the unit cost. Mass concentrated near small distances indicates that correcting node-type distributions primarily involves local adjustments on the graph, whereas diffuse off-diagonal mass implies long-range relocation. As shown in Figures 4 and 5, QW produces a noticeably more localized transport plan than the Base model at the same noise level, consistent with the reduced cost_avg and increased local-mass ratios in Table 6.

G Visualization of Generated Molecular Graphs

We demonstrate some randomly selected molecular graphs generated by TopBF on both QM9 and ZINC250k datasets in Figures. 6 and 7.

H Pseudocode for TopBF

Pseudocode for essential functions in TopBF and continuous-time loss \mathcal{L}_∞ are presented in Algorithms 1 and 2, while sampling procedure is provided in Algorithm 3, wherein NEAREST_CENTER compares the inputs to the nearest centers.

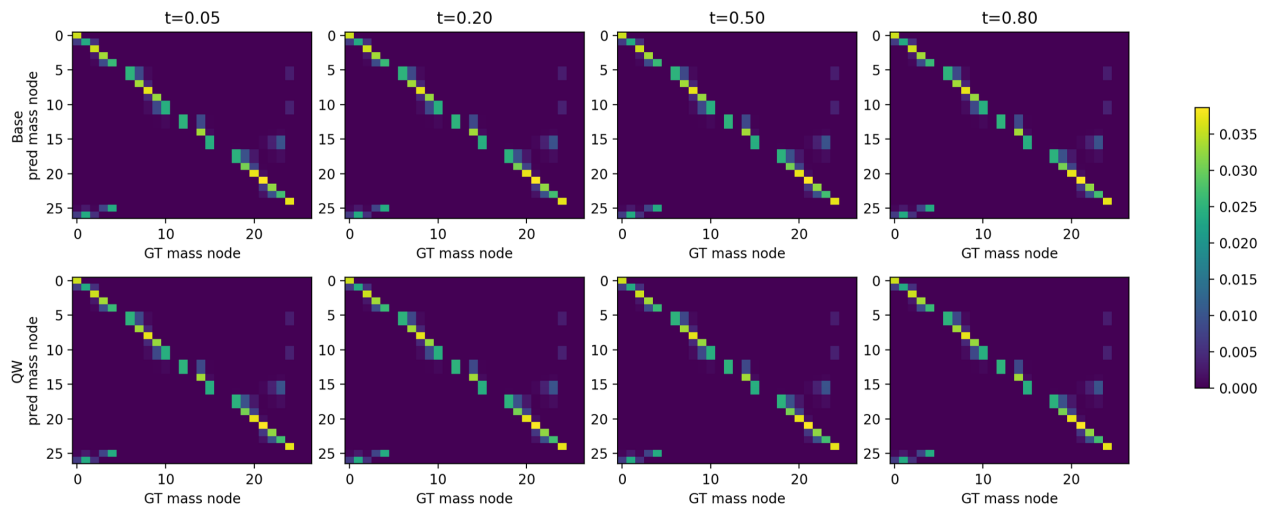


Figure 5: Sinkhorn coupling P between the predicted node-type marginals and the ground truth under the shortest-path (geodesic) cost, probed at $t \in \{0.05, 0.2, 0.5, 0.8\}$ on ZINC250k dataset.

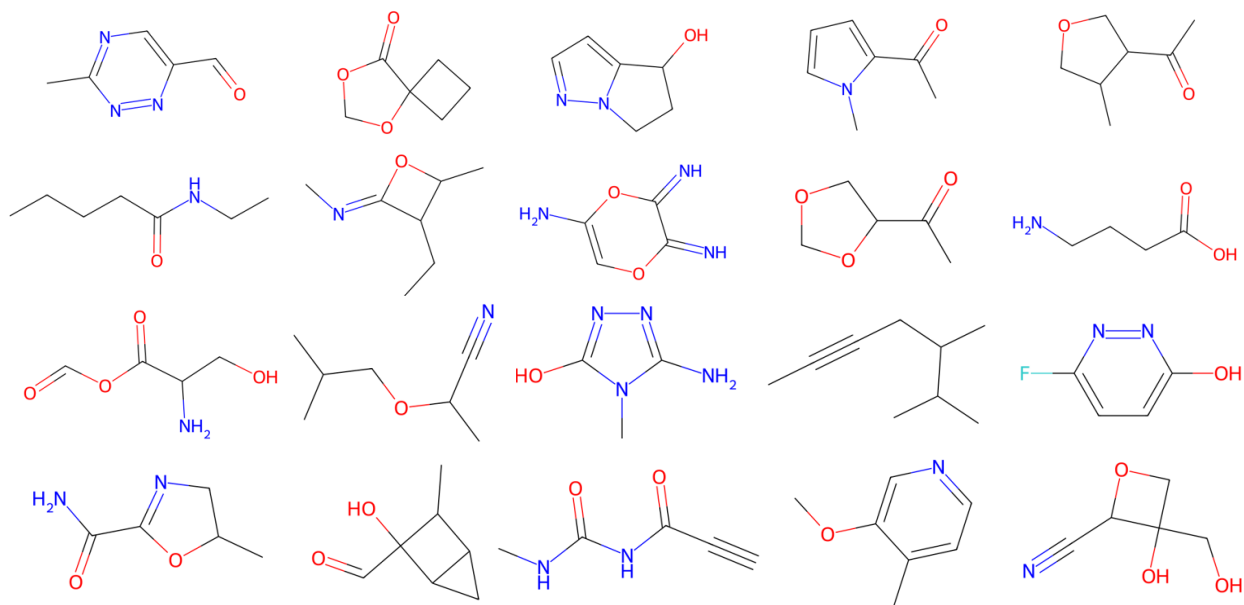


Figure 6: Molecular graphs generated by TopBF on QM9 dataset.

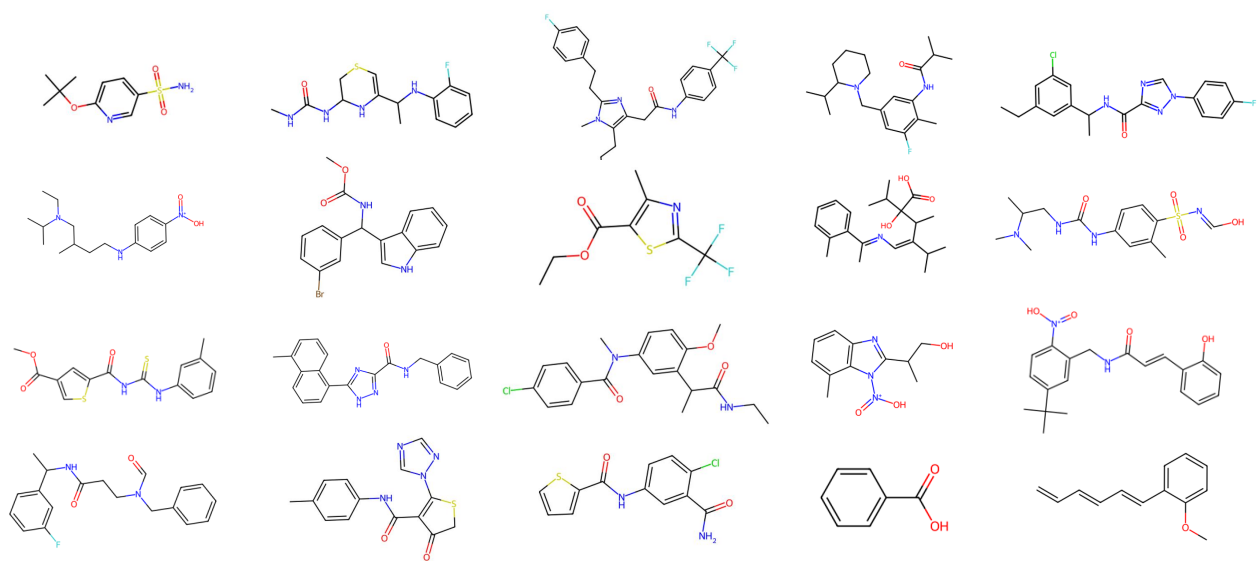


Figure 7: Molecular graphs generated by TopBF on ZINC250k dataset.

Algorithm 1 Functions for TopBF

```
function CDF( $\mu, \sigma, x$ )
 $F(x) \leftarrow \frac{1}{2} \left[ 1 + \operatorname{erf} \left( \frac{x - \mu}{\sqrt{2}\sigma} \right) \right]$ 
if  $x \leq -1$  then
   $H(x) \leftarrow 0$ 
else if  $x \geq 1$  then
   $H(x) \leftarrow 1$ 
else
   $H(x) \leftarrow F(x)$ 
end if
return  $H(x)$ 
end function
function PRED( $\mu \in \mathbb{R}^{D \times K}, t \in [0, 1], K \in \mathbb{N}, \gamma(t) \in \mathbb{R}^+, t_{\min} \in \mathbb{R}^+$ )
#  $t_{\min}$  is set to 0.0001 by default
if  $t < t_{\min}$  then
   $\hat{\mu} \leftarrow 0, \hat{\sigma} \leftarrow 1$ 
else
   $\mu_\epsilon, \ln \sigma_\epsilon \leftarrow \Psi(\boldsymbol{\theta}_t, \mathbf{c}, t)$ 
   $\hat{\mu} \leftarrow \frac{\boldsymbol{\mu}}{\gamma(t)} - \sqrt{\frac{1-\gamma(t)}{\gamma(t)}} \boldsymbol{\mu}_\epsilon$ 
   $\hat{\sigma} \leftarrow \sqrt{\frac{1-\gamma(t)}{\gamma(t)}} \exp(\ln \sigma_\epsilon)$ 
end if
for  $d = 1, \dots, D$  do
  for each  $k \in K$  do
     $p_O^{(d)}(k | \boldsymbol{\theta}) \leftarrow \text{CDF}(\hat{\mu}^{(d)}, \hat{\sigma}^{(d)}, k_r) -$ 
     $\text{CDF}(\hat{\mu}^{(d)}, \hat{\sigma}^{(d)}, k_l)$ 
  end for
end for
return  $p_O(\cdot | \boldsymbol{\theta}_t)$ 
end function
```

Algorithm 2 Training Algorithm

```
Require:  $\sigma_1 \in \mathbb{R}^+, K \in \mathbb{N}$ 
Input: parameterized continuous graph  $\mathbf{G}$ 
 $t \sim \mathcal{U}(0, 1)$ 
 $\gamma \leftarrow 1 - \sigma_1^{2t}$ 
 $\boldsymbol{\mu} \sim \mathcal{N}(\gamma(t), \gamma(t)(1 - \gamma(t))\mathbf{I})$ 
 $p_O(\cdot | \boldsymbol{\theta}_t) \leftarrow \text{PRED}(\boldsymbol{\mu}, t, K, \gamma(t))$ 
 $\hat{\mathbf{k}}_c(\boldsymbol{\theta}_t, t) \leftarrow \text{NEAREST\_CENTER}(p_O(\cdot | \boldsymbol{\theta}_t))$ 
 $\mathcal{L}_\infty(\mathbf{G}) \leftarrow -\ln \sigma_1 \sigma_1^{-2t} \|\mathbf{G} - \hat{\mathbf{k}}_c(\boldsymbol{\theta}_t, t)\|_2^2$ 
return  $\mathcal{L}_\infty(\mathbf{G})$ 
```

Algorithm 3 Sampling Algorithm

```
Require:  $\sigma_1 \in \mathbb{R}^+$ , number of steps  $n, K \in \mathbb{N}$ , optional  $\mathbf{z}^*$ ,
 $\lambda \geq 0$ 
 $\boldsymbol{\mu}_0 \leftarrow \mathbf{0}, \rho_0 \leftarrow 1$ 
for  $i = 1$  to  $n$  do
   $t \leftarrow \frac{i-1}{n}$ 
   $\gamma(t) \leftarrow 1 - \sigma_1^{2t}$ 
   $\boldsymbol{\theta}_t \leftarrow (\boldsymbol{\mu}_{i-1}, \rho_{i-1})$ 
  if  $\mathbf{z}^*$  is not None and  $\lambda > 0$  then
     $\hat{\mathbf{z}}_t \leftarrow R_\varphi(\boldsymbol{\theta}_t, t)$ 
     $\mathcal{L}_{\text{prop}} \leftarrow \|\hat{\mathbf{z}}_t - \mathbf{z}^*\|_2^2$ 
     $\boldsymbol{\mu}_{i-1} \leftarrow \boldsymbol{\mu}_{i-1} - \lambda \nabla_{\boldsymbol{\mu}_{i-1}} \mathcal{L}_{\text{prop}}$ 
     $\boldsymbol{\theta}_t \leftarrow (\boldsymbol{\mu}_{i-1}, \rho_{i-1})$ 
  end if
   $p_O(\cdot | \boldsymbol{\theta}_t) \leftarrow \text{PRED}(\boldsymbol{\mu}_{i-1}, t, K, \gamma(t))$ 
   $\alpha(t) \leftarrow \sigma_1^{-2i/n} (1 - \sigma_1^{2/n})$ 
   $\mathbf{k}_c(\boldsymbol{\theta}_t, t) \leftarrow \text{NEAREST\_CENTER}(p_O(\cdot | \boldsymbol{\theta}_t))$ 
   $\mathbf{Y} \sim \mathcal{N}(\mathbf{k}_c(\boldsymbol{\theta}_t, t), \alpha(t)^{-1}\mathbf{I})$ 
   $\boldsymbol{\mu}_i \leftarrow \frac{\rho_{i-1}\boldsymbol{\mu}_{i-1} + \alpha(t)\mathbf{Y}}{\rho_{i-1} + \alpha(t)}$ 
   $\rho_i \leftarrow \rho_{i-1} + \alpha(t)$ 
end for
 $p_O(\cdot | \boldsymbol{\theta}_1) \leftarrow \text{PRED}(\boldsymbol{\mu}_n, 1, K, 1 - \sigma_1^2)$ 
 $k'_c(\boldsymbol{\theta}_1, 1) \leftarrow \text{NEAREST\_CENTER}(p_O(\cdot | \boldsymbol{\theta}_1))$ 
return  $k'_c(\boldsymbol{\theta}_1, 1)$ 
```
